JBO Journal of Biomedical Optics

RESEARCH PAPER

First in human measurements of abscess cavity optical properties and methylene blue uptake prior to photodynamic therapy by *in vivo* diffuse reflectance spectroscopy

Md Nafiz Hannan,[a] Ashwani K. Sharma,[b] and Timothy M. Baran[b,c,d,*]

[a]University of Rochester, Department of Physics and Astronomy, Rochester, New York, United States
[b]University of Rochester Medical Center, Department of Imaging Sciences, Rochester, New York, United States
[c]University of Rochester, Department of Biomedical Engineering, Rochester, New York, United States
[d]University of Rochester, The Institute of Optics, Rochester, New York, United States

ABSTRACT. **Significance:** Efficacious photodynamic therapy (PDT) of abscess cavities requires personalized treatment planning. This relies on knowledge of abscess wall optical properties, which we report for the first time in human subjects.

Aim: The objective was to extract optical properties and photosensitizer concentration from spatially resolved diffuse reflectance measurements of abscess cavities prior to methylene blue (MB) PDT, as part of a phase 1 clinical trial.

Approach: Diffuse reflectance spectra were collected at the abscess wall of 13 human subjects using a custom fiber-optic probe and optical spectroscopy system, before and after MB administration. A Monte Carlo lookup table was used to extract optical properties.

Results: Pre-MB abscess wall absorption coefficients at 665 nm were $0.15 \pm 0.1\ cm^{-1}$ (0.03 to $0.36\ cm^{-1}$) and $10.74 \pm 15.81\ cm^{-1}$ (0.08 to $49.3\ cm^{-1}$) post-MB. Reduced scattering coefficients at 665 nm were $8.45 \pm 2.37\ cm^{-1}$ (4.8 to $13.2\ cm^{-1}$) and $5.6 \pm 2.26\ cm^{-1}$ (1.6 to $9.9\ cm^{-1}$) for pre-MB and post-MB, respectively. Oxygen saturations were found to be $58.83\% \pm 35.78\%$ (5.6% to 100%) pre-MB and $36.29\% \pm 25.1\%$ (0.0001% to 76.4%) post-MB. Determined MB concentrations were $71.83 \pm 108.22\ \mu M$ (0 to $311\ \mu M$).

Conclusions: We observed substantial inter-subject variation in both native wall optical properties and MB uptake. This underscores the importance of making these measurements for patient-specific treatment planning.

 [DOI: 10.1117/1.JBO.29.2.027002]

Keywords: diffuse reflectance spectroscopy; intra-abdominal abscess; methylene blue; photodynamic therapy; optical properties; hemodynamics

Paper 230310GR received Oct. 2, 2023; revised Feb. 2, 2024; accepted Feb. 6, 2024; published Feb. 27, 2024.

1 Introduction

Abscesses, which consist of a purulent collection surrounded by a fibrous pseudo-capsule, form as a result of host immune and inflammatory response to an acute bacterial infection.[1] These localized pockets of infection can include planktonic microorganisms in the purulent fluid,

*Address all correspondence to Timothy M. Baran, timothy.baran@rochester.edu

as well as biofilm populations growing on the abscess wall. Without treatment, abscess cavities can rupture or spread systemically, leading to high rates of morbidity and mortality.[2] Although image-guided percutaneous drainage has become the standard of care for abscesses that do not respond to antibiotics alone,[3] abscess resolution rates can be low in certain cases[4] and complications following drainage are a persistent problem.[5,6] Even in the case of technically successful drainage, bacteria can remain in the cavity in undrained fluid or as biofilms growing on the abscess wall. The current standard of care therefore relies on antibiotics to eliminate this residual bacterial load. However, the occurrence rate of antibiotic-resistant bacteria is on the rise, with multi-drug resistant pathogens increasingly found in abscess aspirates.[7,8] Alternative treatments are therefore needed.

Photodynamic therapy (PDT), which produces an antimicrobial effect through the photochemical production of reactive oxygen species, may be a powerful adjunct to drainage in the treatment of infected abscesses. Multiple studies have shown that PDT is efficacious *in vitro* against bacterial species that are typically found in abscess cavities.[7,9] Based on these promising results, we completed a phase 1 clinical trial studying the safety and feasibility of PDT with the photosensitizer methylene blue (MB) at the time of abscess drainage (ClinicalTrials.gov Identifier: NCT02240498). The primary clinical outcomes of this trial are reported elsewhere.[8] Here, we focus on the results of optical spectroscopy measurements made immediately prior to PDT.

PDT efficacy is largely determined by the combination of the absorbed light dose and the photosensitizer concentration.[10] The absorbed light dose is determined by the treatment laser power and the optical properties, absorption and scattering, of the target tissue. If the tissue optical properties are known, forward modeling can be used to determine the distribution of light dose within the target tissue. Given a target light dose, patient-specific treatment plans can then be generated to ensure that the entire target region receives an efficacious light dose.

This type of patient-specific PDT treatment planning has been widely applied for interstitial PDT of cancer.[11] For example, Davidson et al. used the treatment diffuser fibers to extract optical properties of the prostate based on a diffusion model.[12] These optical properties were then used to design treatment plans that delivered a threshold dose to the prostate plus margin. Lietke et al. used a similar approach in designing treatment plans for malignant glioma recurrences.[13] In the context of a larger body space, Dupre et al. reported on the performance of surface contact spatially-resolved diffuse reflectance spectroscopy prior to PDT of the pleural cavity.[14] These measurements, along with real-time fluence monitoring,[15] were used to deliver uniform light doses to highly heterogeneous subjects.

While other groups have reported optical property measurements within the human abdomen,[16,17] the optical properties of human abscesses have never been measured, making accurate light dose modeling impossible. To remedy this, we have designed, built, and validated a spatially resolved diffuse reflectance spectroscopy system incorporating multiple optical fibers within a 2 mm outside diameter package.[18,19] As described above, many prior applications typically rely on multiple distinct spectroscopy fibers,[12,13,20] large area of access to the treatment site,[14,15] or bulky, rigid fiber optic probes[21–23] in order to extract patient-specific optical properties for treatment planning. In the case of abscesses, access is generally provided by a small drainage catheter and avoidance of abscess rupture is paramount. The small outside diameter (~2 mm) and flexibility of the fiber-optic probe are therefore crucial for integration into the clinical workflow.

In this study, we performed diffuse reflectance spectroscopy immediately prior to PDT on a series of 13 subjects treated as part of the parent Phase 1 clinical trial. These spectroscopy measurements were taken both before and after MB administration, to quantify native abscess wall optical properties and MB uptake. This represents the first report on the optical properties of human abscess cavities, as well as the retention of MB following a 10 min incubation. These optical property measurements set the stage for patient-specific treatment planning,[24] building on our retrospective study results.[25,26] We previously reported preliminary results for the first three subjects measured in this study.[27] Here, we present the full results for the entire study cohort, including additional analyses.

2 Materials and Methods

2.1 Participants and Regulatory Approval

Spectroscopy data were collected from subjects enrolled in a phase 1 clinical trial examining the safety and feasibility of MB PDT performed at the time of percutaneous abscess drainage (ClinicalTrials.gov Identifier: NCT02240498). The primary results of this clinical trial are reported separately.[8] Of the 18 subjects treated in this trial, optical spectroscopy data were collected from the final 13 subjects as described below. For the first five subjects treated, funding was not available to construct the spectroscopy system described in Sec. 2.2 and perform spectroscopy measurements. All study procedures were approved by the Research Subjects Review Board at the University of Rochester Medical Center, and written informed consent was provided by all subjects.

2.2 Diffuse Reflectance Spectroscopy System

Spatially resolved diffuse reflectance data at the abscess wall were collected using an optical spectroscopy system that was described in detail previously,[18] as shown in Fig. 1(a). Briefly, this system consists of an optical switch (FSM 1x2, Piezosystem Jena, Inc., Hopedale, Massachusetts, United States) that routes either broadband white light (HL-2000-HP-FHSA, Ocean Optics, Inc., Largo, Florida, United States) or laser light at 640 nm (OBIS FP 1193841, Coherent, Inc., Santa Clara, California, United States) to the source fiber on the optical probe displayed in Figs. 1(b) and 1(c). Light transmitted by each of the eight detector fibers is sequentially routed to a spectrometer (QE Pro, Ocean Optics) for detection via another optical switch (FSM 1x8, Piezosystem Jena, Inc.). Detected spectra were corrected for dark background and integration time, and were each divided by a corresponding calibration measurement made using an integrating sphere (3P-GPS-020-SF, Labsphere, Inc., North Sutton, NH) incorporated into the system housing. Details of the calibration procedure are reported elsewhere.[18] While we have examined the fluorescence data collected by this system pre-clinically,[19] the focus of the current study is the analysis of diffuse reflectance data.

The fiber optic probe used for delivery of incident light and detection of diffuse reflectance (Pioneer Optics Company, Bloomfield, Connecticut, United States) is shown in Fig. 1(b). This flexible probe has an outside diameter of 2 mm, to allow it to be inserted through the standard of care drainage catheter used for percutaneous abscess drainage, as described in Sec. 2.3. To determine the source–detector separations necessary for determination of optical properties from measured spectra, images were captured of the probe face using a stereomicroscope with a large working distance (SMZ1500, Nikon Instruments, Inc., Melville, New York, United States). These images were captured with and without a United States Air Force target (USAF 1951 1X, Edmund Optics, Inc., Barrington, New Jersey, United States) in the frame to translate pixel coordinates to distance. These source-detector separations ranged from 320 to 1310 μm, as shown in Fig. 1(c).

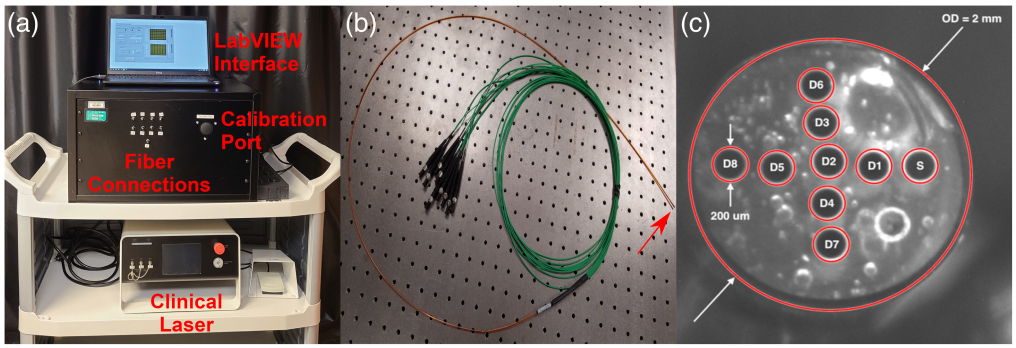

Fig. 1 (a) Image of spectroscopy system showing fiber connections for source and detector fibers, port for integrating sphere calibration, LabVIEW interface, and the laser used for clinical PDT. (b) Image of fiber optic probe, with distal tip indicated by red arrow. (c) Image of fiber optic probe distal face showing the 200 μm diameter fibers used for delivery and detection of light. The source fiber is labeled "S," detector fibers are labeled "D," and outside diameter is abbreviated as "OD."

As described by Bridger et al., these source-detector separations were used to generate a Monte Carlo lookup table for extraction of optical properties from measured spectra.[18] This pre-clinical validation demonstrated root mean square errors of 0.26 to 0.52 μM for MB concentration recovery and 0.86 to 2.7 cm^{-1} for reduced scattering coefficient (μ_s') recovery. This prior publication used a lower resolution color camera to determine fiber positions, whereas the current results utilize the more precise positions determined by microscopic evaluation. Otherwise, the procedure was identical to the previously reported multispectral fitting method. Based on visual inspection of measured spectra, absorption spectra were fit as a superposition of oxy- and deoxy-hemoglobin, MB monomer, and MB dimer absorption spectra. MB dimer absorption was included as MB dimerizes at high concentrations and there is an affiliated change in the absorption spectrum.[28] Reduced scattering spectra were assumed to follow a power-law relationship of the form $\mu_s' = a(\lambda/\lambda_0)^{-b}$, where λ corresponds to wavelength in nm and λ_0 is a normalization wavelength set to 665 nm. Quality of fitting is reported as the sum of root squared error (SRSE) across detector fibers between measured and simulated reflectance spectra.

2.3 Clinical Data Collection

All subjects first had their abscess drained using standard of care image-guided percutaneous drainage, as described in the main trial report.[8] Aspirated fluid was processed by the Clinical Microbiology Laboratory, including identification of isolates and determination of antibiotic susceptibility. Growth of isolates was scored on a semi-quantitative scale ranging from 0 (no growth) to 4+ (heavy growth). The standard of care procedure utilized CT guidance for 16 subjects and ultrasound guidance for 2 subjects. Immediately following drainage, the cavity was first flushed twice with sterile saline. The disinfected optical probe was then removed from the bag and the proximal fiber ends connected to the spectroscopy system. The distal end was then held in place at the entrance port of the system integrating sphere by the interventional radiologist. Calibration spectra were captured at each detector fiber for both broadband and laser illumination, with an integration time of 100 ms for broadband illumination and 50 ms for laser illumination. These calibration spectra were used to correct patient data as described in Sec. 2.2.

In order to measure patient optical properties, the interventional radiologist advanced the optical probe through the standard of care drainage catheter until it made gentle contact with the abscess wall. Surface contact was insured through tactile feedback by the study doctor, and by monitoring the signal detected at the closest detector fiber in real time. As described by Chen et al.,[29] detected reflectance increases as the probe approaches the surface before rapidly decreasing when surface contact is made. This is due to the transition from specular to diffuse reflectance.

Once surface contact was made, diffuse reflectance and fluorescence spectra were captured at each detector fiber sequentially. For each fiber, an initial integration time of 50 ms was used. Assuming a linear relationship between integration time and detected signal, the maximum magnitude of the detected signal was used to calculate the integration time that would result in 50% of the dynamic range of the spectrometer being utilized. This was chosen to compromise between signal to noise ratio and measurement time. A measurement was then performed at this calculated integration time. Dark spectra were also collected at this point as described in Sec. 2.2 using the same integration times by disabling the source switch. If the captured spectra were not of sufficient quality, the probe was withdrawn and replaced by the study doctor, and spectroscopy was repeated. This measurement was meant to capture native abscess wall optical properties prior to MB infusion and is referred to as the "pre-MB" measurement elsewhere.

Following this, 0.1% MB (BPI Labc, LLC, Largo, Florida, United States) was infused into the abscess cavity and incubated for 10 min to allow for bacterial uptake. A 10 min incubation interval was selected based on prior reports of *in vitro* PDT efficacy against multiple bacterial isolates from human abscess aspirates using this incubation time.[7] This short interval was also selected to improve specificity of MB uptake, based on the rapid internalization of cationic photosensitizers by bacteria relative to host cells.[30] MB was then aspirated and the cavity was flushed twice with sterile saline for all subjects. The optical probe was then re-inserted through the drainage catheter into gentle contact with the abscess wall, and measurements were repeated as described above. This measurement was meant to capture the uptake of MB and is referred to as the "post-MB" measurement throughout.

After the completion of optical spectroscopy measurements, the optical probe was removed and PDT was performed as described in the main clinical trial report.[8] This consisted of an infusion of a lipid emulsion to scatter treatment light through the irregular abscess cavity, insertion of a sterile optical fiber, and delivery of laser light at 665 nm.

2.4 Data Processing

As described above, collected spectra were corrected for dark background and integration time, and divided by corresponding spectra collected at the entrance port of the system integrating sphere. Optical property spectra were extracted using the Monte Carlo lookup table approach described in Sec. 2.2. Whereas pre-clinical validation of the system used all eight detector fibers, high-quality data could not be collected at all detector fibers for all subjects in clinical measurements. This was mainly due to poor surface contact between specific detector fibers and the abscess wall, even after repositioning of the optical probe. Additionally, for subjects with high MB uptake, spectra collected at larger source-detector separations did not have sufficient signal to noise ratio for analysis due to major attenuation by MB absorption. In cases where spectra at individual detectors were not usable, these detected fibers were excluded from the optical property inversion. As we have shown previously, utilization of fewer source-detector separations does not significantly impact the accuracy of optical property recovery, as long as data from at least 4-5 detector fibers are included.[31,32] This was achievable for all but the first subject, resulting in 13 pre-MB measurements and 12 matched post-MB measurements.

2.5 Statistical Analysis

Continuous values are summarized across subjects as mean $\pm$ standard deviation, whereas categorical values are summarized as proportions with 95% confidence intervals. Demographic information was compared between the 13 subjects that received optical spectroscopy and the five treated prior to construction of the optical spectroscopy system using the Mann–Whitney test for continuous variables and Fisher's exact test for categorical values. Extracted optical properties at 665 nm and SO_2 were compared between pre- and post-MB measurements using the Wilcoxon signed-rank test. Correlation between MB concentration and change in SO_2 was calculated using the Spearman correlation coefficient. Optical properties were compared between abscess locations using the Kruskal–Wallis test, with Dunn's test for pairwise comparisons. The Mann–Whitney test was used to compare MB concentration between those with heavy bacterial growth reported for their standard of care abscess aspirate (4+) to those with less growth (<4). A p value less than 0.05 was considered significant, and all analyses were performed in GraphPad PRISM (v6, GraphPad Software, Inc., San Diego, California, United States) and MATLAB (R2022b, The Mathworks, Inc., Natick, Massachusetts, United States).

3 Results

3.1 Subject Demographics

Subject demographics for all subjects that received PDT, as well as separated by whether optical spectroscopy measurements were made, are included in Table 1. As can be seen, there were no significant differences in demographics between subjects that did and did not receive optical spectroscopy. For the 13 subjects described in this report, 38.5% were male and the average age was 56.9 ± 20.3 years.

3.2 Representative Data from Two Subjects

Representative diffuse reflectance spectra for two subjects are shown in Fig. 2, with fully corrected data shown as open circles and best fit spectra shown as solid lines. As can be seen in Figs. 2(a) and 2(c), pre-MB data were accurately fit with a super-position of oxy- and deoxy-hemoglobin absorption and power-law reduced scattering. Post-MB data, as shown in Figs. 2(b) and 2(d), were well fit by the addition of MB monomer and dimer spectra.

These fits were used to extract the optical property spectra shown in Fig. 3. As can be seen, there was variability between subjects in both pre-MB optical properties and MB uptake. Figures 3(a) and 3(c) demonstrate large differences in absorption spectra between subjects for

Table 1 Subject demographics for overall sample and separated by whether spectroscopy was performed.

	Overall sample ($n = 18$)	Optical spectroscopy performed ($n = 13$)	Optical spectroscopy not performed ($n = 5$)	P value
Age	60.1 ± 18.3	56.9 ± 20.3	68.6 ± 7.6	0.20
Sex (% male)	44.4% (21.5% to 69.2%)	38.5% (13.9% to 68.4%)	60.0% (14.7% to 94.7%)	0.61
BMI	29.3 ± 5.9	30.0 ± 6.3	25.4 ± 6.1	0.39
Abscess volume (mL)	36.8 ± 40.6	25.2 ± 22.0	67.0 ± 63.0	0.18

P values are the results of the Mann–Whitney test for continuous variables and Fisher's exact test for categorical variables, comparing those for which optical spectroscopy was and was not performed.

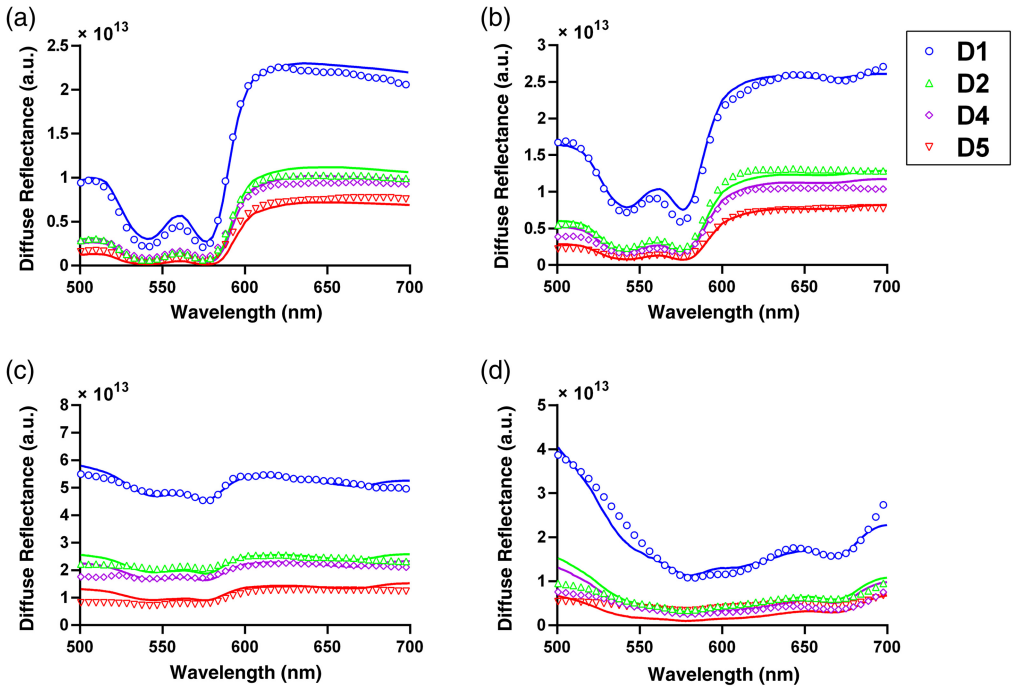

Fig. 2 Corrected diffuse reflectance data (open circles) and fits (solid line) for detector fibers 1, 2, 4, and 5 for subject 3 (a) pre-MB (SRSE $= 1.18 \times 10^{15}$) and (b) post-MB (SRSE $= 1.13 \times 10^{15}$), and subject 8 (c) pre-MB (SRSE $= 1.32 \times 10^{15}$) and (d) post-MB (SRSE $= 1.36 \times 10^{15}$). Colors and symbols indicate different detector fibers.

both pre-MB and post-MB conditions. In both subjects, oxy- and deoxy-hemoglobin were the main absorbers.

In the post-MB condition for subject 3, oxy- and deoxy-hemoglobin remained the dominant absorbers. For subject 8, MB monomer and dimer dominated the post-MB absorption spectra, with some contributions from oxy- and deoxy- hemoglobin. Figures 3(b) and 3(d) illustrate notable differences in reduced scattering spectra between subjects for pre-MB and post-MB conditions.

3.3 Native Abscess Wall Optical Properties

Native, pre-MB abscess wall optical properties at 665 nm across subjects are tabulated in Table 2. Substantial inter-patient variability in native abscess-wall optical properties and oxygen saturation were observed (Fig. 4). Means and standard deviations for absorption coefficient at 665 nm

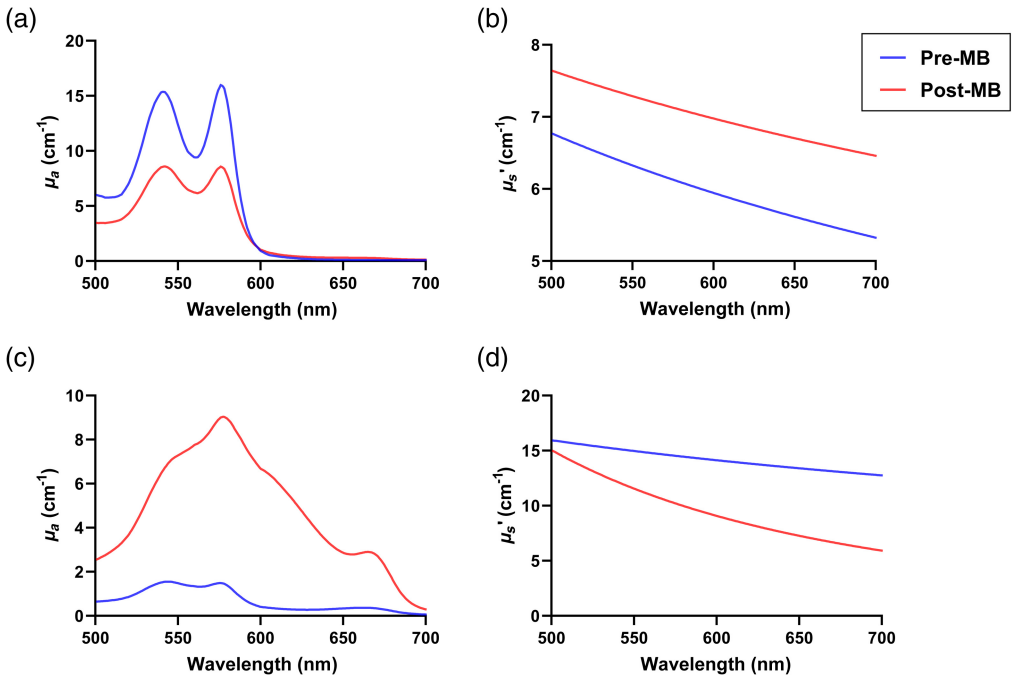

Fig. 3 Recovered (a) absorption (μ_a) and (b) reduced scattering (μ_s') spectra for subject 3 shown in Figs. 2(a) and 2(b). Recovered (c) μ_a and (d) μ_s' spectra for subject 8 shown in Figs. 2(c) and 2(d). Blue and red lines represent pre-MB and post-MB conditions, respectively.

Table 2 Extracted optical properties at 665 nm and oxygen saturation for each subject, before and after addition of methylene blue (MB). MB concentration ([MB]) is also included for post-MB measurements.

	Pre-MB			Post-MB			
Subject number	$\mu_{a,665}$ (cm^{-1})	$\mu_{s,665}'$ (cm^{-1})	SO_2 (%)	$\mu_{a,665}$ (cm^{-1})	$\mu_{s,665}'$ (cm^{-1})	SO_2 (%)	[MB] (μM)
1[a]	0.32	6.7	100.0	—	—	—	—
2	0.03	10.6	56.5	9.6	9.8	7.6	58.2
3	0.09	5.5	100.0	0.28	6.6	76.4	0.8
4	0.14	7.1	81.1	10.1	4.0	45.5	59.4
5	0.11	8.6	81.4	3.1	1.6	45.1	1.7×10^{-6}
6	0.09	4.8	87.7	49.4	3.4	36.3	311
7	0.21	8.7	17.4	0.08	9.9	72.4	0
8	0.36	13.2	48.7	2.9	6.8	29.9	8.0
9	0.14	10.4	100.0	5.0	4.1	23.7	13.2
10	0.20	7.2	8.4	3.6	3.5	40.0	17.1
11	0.06	7.6	54.2	41.5	4.5	20.3	227
12	0.11	11.3	5.6	0.86	6.5	0.0001	4.3
13	0.04	8.0	23.8	1.76	3.2	37.7	7.0

[a]Post-MB data were not of sufficient quality for interpretation for subject 1.

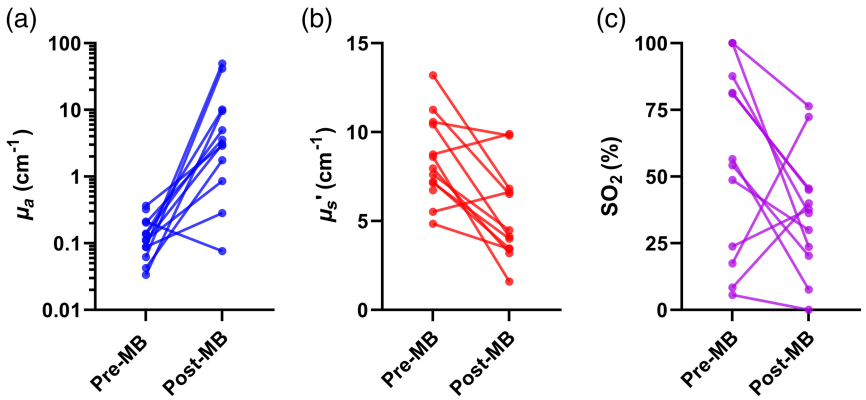

Fig. 4 Extracted (a) absorption coefficients (μ_a) at 665 nm, (b) reduced scattering coefficients (μ_s') at 665 nm, and (c) oxygen saturation (SO_2) for all subjects for pre-MB and post-MB conditions. Note that (a) is on a log scale, and (b) and (c) are on linear scales.

($\mu_{a,665}$) were 0.15 ± 0.1 cm^{-1} (range: 0.03 to 0.36 cm^{-1}), and 8.45 ± 2.37 cm$-^{1}$ (range: 4.8 to 13.2 cm^{-1}) for reduced scattering coefficient at 665 nm ($\mu'_{s,665}$). Oxygen saturation (SO_2) was found to be $58.83\% \pm 35.78\%$ (range: 5.6% to 100%).

3.4 Methylene Blue Uptake and Changes in Extracted Optical Properties

Measured MB concentrations across subjects are tabulated in Table 2. Mean and standard deviation for this was 71.83 ± 108.22 μM (range: $0 - 311$ μM), which reveals substantial inter-patient variation. As expected, there was a significant increase in μ_a at 665 nm for post-MB measurements ($p = 0.001$), due to the presence of MB absorption [Fig. 4(a)]. There was also an apparent decrease in μ_s' at 665 nm [$p = 0.005$, Fig. 4(b)]. While there was a decrease in SO_2 from pre- to post-MB values [median reduction = 28.8%, Fig. 4(c)], this difference was not significant ($p = 0.11$). Additionally, this change in SO_2 from pre- to post-MB measurement was not significantly correlated with measured MB concentration ($\rho = 0.49$, $p = 0.11$). There was also no significant difference in MB concentration between those subjects graded as having heavy growth on their standard of care abscess aspirate (4+ as reported by the Clinical Microbiology Laboratory) and those with less than heavy growth (4+: 32.2 ± 30.7 μM, <4: 68.1 ± 120.8 μM; $p = 0.81$).

As the fiber optic probe was removed and reinserted between the pre- and post-MB data collection, some of this variability may also represent small differences in the exact placement of the probe face. Due to clinical time constraints, we were unable to perform repeated measurements to assess variability due to probe placement. This will be an important piece of future studies.

3.5 Differences based on Abscess Location or Bacteria Present

For the 13 abscesses that were quantified optically, four were located in the pelvis, five were associated with the colon, and four were found in other locations. While sample sizes were small, we performed preliminary analysis to examine regional differences in optical properties. None of the quantities reported in Table 2 were found to be significantly different between these rough location groupings.

Of the bacterial species found in abscesses measured, the most common was *Escherichia coli* (*E. coli*, $n = 3$). Other abscess cavities were found to contain a variety of other species. While abscess containing *E. coli* tended to have higher MB uptake than those with other bacterial species (97.7 ± 114.7 μM versus 14.8 ± 22.7 μM), this difference was not statistically significant ($p = 0.17$). Four of the 13 abscesses measured were found to contain antibiotic-resistant bacterial strains. MB uptake was not different between strains that were resistant or susceptible to antibiotics ($p = 0.63$), indicating that PDT susceptibility in antibiotic-resistant strains would not be limited by MB concentration.

4 Discussion and Conclusion

We performed clinical spatially resolved diffuse reflectance spectroscopy of human abscess cavities prior to PDT, representing the first time that the optical properties of human abscesses have been quantified. There was substantial variation in the native abscess wall optical properties prior to MB administration, particularly in absorption at 665 nm and SO_2. Uptake of MB, as measured by post-MB diffuse reflectance, varied widely between subjects. Infusion of MB appeared to reduce SO_2 measured at the abscess wall, with minimal effects on tissue scattering. There were no significant differences based on abscess location or bacteria present. These observations motivate future studies focused on the underlying causes of these observed heterogeneities, particularly for MB uptake.

This represents the first study that measured the optical properties of human abscesses. As such, direct comparisons to perfectly analogous results are impossible. However, other investigators have reported optical properties measured within nearby anatomy in the abdomen. Perhaps the most thorough of these is Morales et al., where diffuse reflectance measurements were made with a surface-contact probe throughout the peritoneal cavity.[16] This included measurements at the surface of multiple organs, the chest wall, and skin. Pre-MB absorption and reduced scattering coefficients determined in this study fall within the ranges reported by these investigators. Wang et al. also measured optical properties within the peritoneal cavity prior to PDT.[33] Although their results are provided at 630 nm rather than 665 nm, our reported values are similar to those reported for the peritoneum, small bowel, and large bowel. We have also previously measured the optical properties of excised human kidneys,[31] finding that absorption and reduced scattering at 665 nm ranged from 0.3 to 1.7 cm^{-1} and 12.5 to 39.4 cm^{-1}, respectively. These ranges are again similar to what we find in the present study. Abscesses are not routinely surgically excised, as this significantly increases morbidity and mortality.[34] Capture of biopsy samples is also not possible, as this could rupture the cavity and lead to sepsis. We therefore do not have patient tissue available to perform optical property quantification via other means. Based on these other reports, however, it appears that our measurements are in reasonable concordance with similar abdominal tissue. Future studies will include repeated measurements for the same subject, to evaluate optical property homogeneity and variability in the measurement and fitting process.

Oxygen saturation (SO_2), as determined by the relative concentrations of oxy- and deoxy-hemoglobin, was found to decrease from the pre- to post-MB measurements ($55.4\% \pm 35.1\%$ versus $36.2\% \pm 22.7\%$) and this decrease was correlated with measured MB concentration ($\rho = 0.49$). However, this change was not statistically significant ($p = 0.11$). This suggests that the infusion of a high MB concentration, even after flushing the cavity with sterile saline, may be related to a reduction in SO_2. One potential explanation is localized oxidation of hemoglobin to methomoglobin, which cannot bind oxygen,[35] at high MB concentrations.[36] As we rely on the balance between oxy- and deoxy-hemoglobin to determine SO_2, any changes in the ability of hemoglobin to bind oxygen would be incorrectly interpreted as a reduction in the availability of oxygen. Other studies have shown that systemic administration of MB can also result in artificially low SO_2 readings on standard pulse oximetry.[37–39] This could be examined further by including *in situ* measurements with an oxygen-sensitive microelectrode, as we have done previously in phantom studies.[40] Importantly, we did not observe changes in SO_2 with standard of care pulse oximetry on the finger, indicating that these changes are localized to the region of MB administration.

As described in Sec. 2.2, we use a multispectral fitting procedure that includes absorption contributions from hemoglobin (oxy- and deoxy-) and MB (monomer and dimer). For the range of MB concentrations we observed here, the inclusion of MB dimer absorption was of particular importance for post-MB measurements. MB forms dimers in aqueous solution, with the dimer fraction correlated with MB concentration.[41] The absorption of this dimer is shifted from the monomer peak of 664 nm to approximately 600 nm. In addition to more accurate fitting in the spectral region around 600 nm, the inclusion of MB dimer absorption also had a profound effect on the accuracy of SO_2 determination. An example of this is shown in Fig. 5. Without the MB dimer in the fit the spectral shape is not fit well and an erroneously low SO_2 value is returned. When the MB dimer is properly included [see Fig. 2(d)], the fit is of much higher quality and the correct value of SO_2 is found. For the example shown in Fig. 5, the SO_2 value increased from 0% to 29.9% by inclusion of the dimer. Across all subjects, if fits were performed with the MB dimer

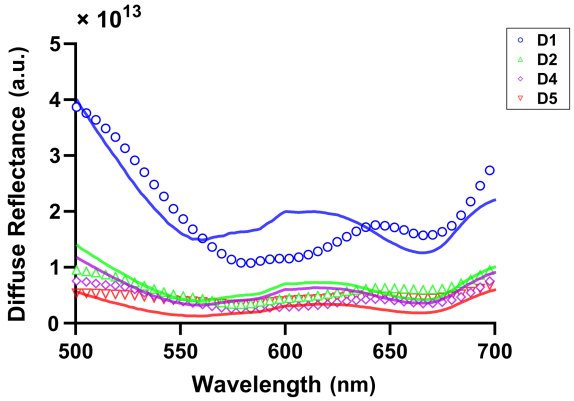

Fig. 5 Effect of excluding MB dimer from fitting for the same subject shown in Fig. 2(d). Colors and symbols represent different detector fibers.

absorption included, the determined SO_2 post-MB was significantly increased (36.2% ± 22.7% versus 25.9% ± 27.3%, $p = 0.027$). This highlights the importance of incorporating all relevant absorbers into spectral fitting.

As mentioned previously, MB dimer formation generally occurs at high MB concentration. Taken together with the observation of negative correlation between MB uptake and SO_2, this motivates reduction of MB concentration in future studies. This is further supported by preclinical studies, where MB concentration is typically much lower than the 1 mg/mL concentration used here. For example, Haidaris et al. showed efficacious PDT against multiple bacterial species isolated from patient abscess aspirates at a MB concentration of 300 μg/mL.[7] In an *in vivo* study in cows, Sellera et al. showed that a MB concentration of 100 μg/mL (0.01%) was efficacious in treating bovine skin infection when combined with red light-emitting diode (LED) illumination.[42] This 0.01% (100 μg/mL) MB concentration was also shown to be efficacious in controlling *Streptococcus mutans* biofilms.[43] For clinical studies of MB-PDT, concentrations ranging from 25 to 100 μg/mL have typically been reported,[44–46] with some investigators using higher concentrations for topical application.[47] However, these studies using higher concentrations typically employ much higher fluence rates,[48] which are not applicable in the case of abscesses.

The wide variability in extracted optical properties, particularly after the addition of MB, provides a strong motivation for the performance of patient-specific treatment planning in future PDT of abscesses. In prior retrospective studies, we have shown the importance of this for improving eligibility for PDT.[25,26] Further, the optical properties reported here have been used to generate retrospective treatment plans for the 13 subjects that received both PDT and spectroscopy.[24] In particular, the effects of abscess wall absorption have a pronounced effect on generated treatment plans. Along with the evidence discussed above, this motivates a reduction in MB concentration in future studies. While prior studies in oncological PDT have employed patient-specific treatment planning,[11–13] none of these studies have directly compared patient-specific treatment plans to "fixed dose" plans that do not incorporate patient-specific optical properties. This motivates a direct comparison between a "fixed dose" case and patient-specific treatment planning in upcoming clinical trials.

We acknowledge some limitations in the present study. These findings are from a relatively small ($n = 13$) group of subjects treated with PDT at the time of their abscess drainage, so results could be vulnerable to bias. While a large number of the abscesses measured presented in the pelvis ($n = 4$), many were located in other anatomical locations. There is therefore insufficient sample size to make conclusive statements about regional differences in optical properties. Additionally, extraction of optical properties required the fiber optic probe to make surface contact with the abscess wall. While we used both tactile and optical feedback to verify this, it was apparent in some cases that certain detector fibers were not in contact with the abscess wall. This meant that extraction of optical properties in these cases was based upon a smaller number of detector fibers, which could reduce precision. Further, measurements were only performed at a single location on the abscess wall. These factors motivate the design of alternate probe geometries for future studies, as well as evaluation of the spatial heterogeneity of optical properties and

MB uptake. Also, although the saline flushing procedure after MB incubation was identical between subjects, the concentration of MB in extracted saline was not directly measured. This would have provided confirmation that observed differences in apparent MB uptake were not due to the saline flushing process. Future studies will capture the extracted saline after flushing, in order to control for this factor. Finally, while measurements were made before and after the addition of MB, no measurements were made after PDT. This has been done by other groups for PDT of cancer,[16,49] to quantify photosensitizer bleaching and PDT-induced changes in optical properties.

Disclosures

The authors have no conflicts of interest to disclose.

Code and Data Availability

The data that support the findings of this article are not publicly available due to privacy concerns, as research subjects did not consent to use of their data beyond the purposes of this study.

Acknowledgments

The authors would like to thank Dr. Joan Adamo, Laurie Christensen, Erica Longbine, and Maria Favella for regulatory support. This work was funded by grant EB029921 from the National Institutes of Health.

References

1. S. D. Kobayashi, N. Malachowa, and F. R. DeLeo, "Pathogenesis of *Stapylococcus aureus* abscesses," *Am. J. Pathol.* **185**, 1518–1527 (2015).
2. S. Men, O. Akhan, and M. Köroğlu, "Percutaneous drainage of abdominal abscess," *Eur. J. Radiol.* **43**, 204–218 (2002).
3. T. A. Jaffe and R. C. Nelson, "Image-guided percutaneous drainage: a review," *Abdom. Radiol.* **41**, 629–636 (2016).
4. E. vanSonnenberg et al., "Percutaneous abscess drainage: update," *World J. Surg.* **25**, 362–369 (2001).
5. M. S. Gee et al., "Management of abdominal and pelvic abscesses that persist despite satisfactory percutaneous drainage catheter placement," *AJR Am. J. Roentgenol.* **194**, 815–820 (2010).
6. D. A. Gervais et al., "Recurrent abdominal and pelvic abscesses: incidence, results of repeated percutaneous drainage, and underlying causes in 956 drainages," *AJR Am. J. Roentgenol.* **182**, 463–466 (2004).
7. C. G. Haidaris et al., "Effective photodynamic therapy against microbial populations in human deep tissue abscess aspirates," *Lasers Surg. Med.* **45**, 509–516 (2013).
8. T. M. Baran et al., "Photodynamic therapy is a safe and feasible adjunct to percutaneous drainage of deep tissue abscesses: results of a first in humans Phase 1 clinical trial," medRxiv 2023.10.16.23297086 (2023).
9. H. Chan, M. S. Pavelka, and T. M. Baran, "Methylene blue photodynamic therapy of bacterial species found in human abscesses: planktonic, biofilm, and 3D silicone models," *Proc. SPIE* **12358**, 1235805 (2023).
10. B. C. Wilson, M. S. Patterson, and L. Lilge, "Implicit and explicit dosimetry in photodynamic therapy: a new paradigm," *Lasers Med. Sci.* **12**, 182–199 (1997).
11. G. Shafirstein et al., "Interstitial photodynamic therapy—a focused review," *Cancers* **9**, 12 (2017).
12. S. R. H. Davidson et al., "Treatment planning and dose analysis for interstitial photodynamic therapy of prostate cancer," *Phys. Med. Biol.* **54**, 2293–2313 (2009).
13. S. Lietke et al., "Interstitial photodynamic therapy using 5-ALA for malignant glioma recurrences," *Cancers* **13**, 1767 (2021).
14. P. J. Dupre et al., "Light fluence rate and tissue oxygenation (StO2) distributions within the thoracic cavity of patients receiving intraoperative photodynamic therapy for malignant pleural mesothelioma," *Photochem. Photobiol.* **96**, 417–425 (2020).
15. M. M. Kim et al., "Infrared navigation system for light dosimetry during pleural photodynamic therapy," *Phys. Med. Biol.* **65**, 075006 (2020).
16. R. D. H. Morales et al., "In vivo spectroscopic evaluation of human tissue optical properties and hemodynamics during HPPH-mediated photodynamic therapy of pleural malignancies," *J. Biomed. Opt.* **27**, 105006 (2022).
17. S. L. Jacques, "Optical properties of biological tissues: a review," *Phys. Med. Biol.* **58**, R37 (2013).

18. K. G. Bridger, J. R. Roccabruna, and T. M. Baran, "Optical property recovery with spatially-resolved diffuse reflectance at short source-detector separations using a compact fiber-optic probe," *Biomed. Opt. Express* **12**, 7388–7404 (2021).
19. J. Roccabruna, K. Bridger, and T. Baran, "Fluorescence and diffuse reflectance provide similar accuracy in recovering fluorophore concentration at short source-detector separations," *J. Mod. Opt.* **69**, 699–704 (2022).
20. J. Swartling et al., "System for interstitial photodynamic therapy with online dosimetry: first clinical experiences of prostate cancer," *J. Biomed. Opt.* **15**, 058003 (2010).
21. E. J. M. Baltussen et al., "Diffuse reflectance spectroscopy as a tool for real-time tissue assessment during colorectal cancer surgery," *J. Biomed. Opt.* **22**, 106014 (2017).
22. P. Naglič et al., "Estimation of optical properties by spatially resolved reflectance spectroscopy in the subdiffusive regime," *J. Biomed. Opt.* **21**, 095003 (2016).
23. D. J. Carpenter et al., "Noninvasive optical spectroscopy for identification of non-melanoma skin cancer: pilot study," *Lasers Surg. Med.* **50**, 246–252 (2018).
24. Z. Li et al., "Treatment planning for photodynamic therapy of abscess cavities using patient-specific optical properties measured prior to illumination," medRxiv 2023.10.23.23297420 (2023).
25. T. M. Baran et al., "Photodynamic therapy of deep tissue abscess cavities: Retrospective image-based feasibility study using Monte Carlo simulation," *Med. Phys.* **46**, 3259–3267 (2019).
26. Z. Li et al., "Effects of patient-specific treatment planning on eligibility for photodynamic therapy of deep tissue abscess cavities: retrospective Monte Carlo simulation study," *J. Biomed. Opt.* **27**, 083007 (2022).
27. M. N. Hannan, A. K. Sharma, and T. M. Baran, "Preliminary measurements of optical properties in human abscess cavities prior to methylene blue photodynamic therapy," *Proc. SPIE* **12359**, 123590A (2023).
28. K. Bergmann and C. T. O'Konski, "A spectroscopic study of methylene blue monomer, dimer, and complexes with montmorillonite," *J. Phys. Chem.* **67**, 2169–2177 (1963).
29. W. Chen et al., "Influence of contact state on NIR diffuse reflectance spectroscopy in vivo," *J. Phys. D Appl. Phys.* **38**, 2691 (2005).
30. T. Dai, Y.-Y. Huang, and M. R. Hamblin, "Photodynamic therapy for localized infections—state of the art," *Photodiagn. Photodyn. Ther.* **6**, 170–188 (2009).
31. T. M. Baran et al., "Optical property measurements establish the feasibility of photodynamic therapy as a minimally invasive intervention for tumors of the kidney," *J. Biomed. Opt.* **17**, 098002 (2012).
32. T. M. Baran, "Improved tissue optical property extraction at short source-detector separations using neural networks," in *Front. in Opt. + Laser Sci. (FIO, LS)*, Optica Publishing Group, p. FTh3B.2 (2022).
33. H.-W. Wang et al., "Broadband reflectance measurements of light penetration, blood oxygenation, hemoglobin concentration, and drug concentration in human intraperitoneal tissues before and after photodynamic therapy," *J. Biomed. Opt.* **10**, 014004 (2005).
34. A. D. Politano et al., "Differences in morbidity and mortality with percutaneous versus open surgical drainage of postoperative intra-abdominal infections: a review of 686 cases," *Am. Surg.* **77**, 862–867 (2011).
35. C. M. McRobb and D. W. Holt, "Methylene blue-induced methemoglobinemia during cardiopulmonary bypass? A case report and literature review," *J. Extra Corpor. Technol.* **40**, 206–214 (2008).
36. S. R. David et al., "The blood blues: a review on methemoglobinemia," *J. Pharmacol. Pharmacother.* **9**, 1–5 (2018).
37. J. J. Kirlangitis et al., "False indication of arterial oxygen desaturation and methemoglobinemia following injection of methylene blue in urological surgery," *Military Med.* **155**, 260–262 (1990).
38. A. Sidi et al., "Methylene blue and indocyanine green artfactually lower pulse oximetry readings of oxygen saturation. Studies in dogs," *J. Clin. Monitor.* **3**, 249–256 (1987).
39. L. Q. Rong et al., "Characterization of the rapid drop in pulse oximetry reading after intraoperative administration of methylene blue in open thoracoabdominal aortic repairs," *Anesth. Analg.* **129**, e142–e145 (2019).
40. T. M. Baran, M. C. Fenn, and T. H. Foster, "Determination of optical properties by interstitial white light spectroscopy using a custom fiber optic probe," *J. Biomed. Opt.* **18**, 107007 (2013).
41. M. N. Usacheva, M. C. Teichert, and M. A. Biel, "The role of the methylene blue and toluidine blue monomers and dimers in the photoinactivation of bacteria," *J. Photochem. Photobiol. B Biol.* **71**, 87–98 (2003).
42. F. P. Sellera et al., "Methylene blue-mediated antimicrobial photodynamic therapy can be a novel non-antibiotic platform for bovine digital dermatitis," *Photodiagn. Photodyn. Ther.* **34**, 102274 (2021).
43. M. A. Nemezio et al., "Effect of methylene blue-induced photodynamic therapy on a Streptococcus mutans biofilm model," *Photodiagn. Photodyn. Ther.* **20**, 234–237 (2017).
44. N. Derikvand et al., "Antimicrobial photodynamic therapy with diode laser and methylene blue as an adjunct to scaling and root planning: a clinical trial," *Photodiagn. Photodyn. Ther.* **31**, 101818 (2020).
45. R. G. D. Miranda and A. P. V. Colombo, "Clinical and microbiological effectiveness of photodynamic therapy on primary endodontic infections: a 6-month randomized clinical trial," *Clin. Oral Investig.* **22**, 1751–1761 (2018).
46. L. H. Alvarenga et al., "Parameters for antimicrobial photodynamic therapy on periodontal pocket—randomized clinical trial," *Photodiagn. Photodyn. Ther.* **27**, 132–136 (2019).

47. R. B. Cecatto et al., "Methylene blue mediated antimicrobial photodynamic therapy in clinical human studies: the state of the art," *Photodiagn. Photodyn. Ther.* **31**, 101828 (2020).
48. E. Alberdi and C. Gómez, "Efficiency of methylene blue-mediated photodynamic therapy vs intense pulsed light in the treatment of onychomycosis in the toenails," *Photodermatol. Photoimmunol. Photomed.* **35**, 69–77 (2019).
49. T. A. Middelburg et al., "Correction for tissue optical properties enables quantitative skin fluorescence measurements using multi-diameter single fiber reflectance spectroscopy," *J. Dermatol. Sci.* **79**, 64–73 (2015).

Md Nafiz Hannan is a PhD student in the Department of Physics and Astronomy at the University of Rochester. He received his BS degree in physics and industrial engineering from Shahjalal University of Science and Technology in 2018 and his MA degree in physics from the University of Rochester in 2023. His research interest includes optical spectroscopy and imaging, photodynamic therapy, and machine learning.

Ashwani K. Sharma is an associate professor of imaging sciences at the University of Rochester Medical Center. He received his medical degree at Maulana Azad Medical College, and performed fellowship at the University of Rochester Medical Center. He is a board-certified interventional radiologist and is the director of interventional oncology in Imaging Sciences. His research interests include use of radiopharmaceuticals for hepatic tumors, photodynamic therapy, and transplant interventions.

Timothy M. Baran is an assistant professor of imaging sciences and biomedical engineering at the University of Rochester, with a secondary appointment in The Institute of Optics. He received his BS degree in electrical, computer, and systems engineering from Rensselaer Polytechnic Institute in 2007 and his PhD in optics from the University of Rochester in 2013. His research interests include diffuse optical spectroscopy, photodynamic therapy, and medical image processing.